Inverse Estimation of Front Surface Temperature of a Plate with Laser Heating and Convection-Radiation Cooling

Jianhua Zhou, Yuwen Zhang[1], J. K. Chen and Z. C. Feng

Department of Mechanical and Aerospace Engineering, University of Missouri, Columbia, MO 65211, USA

The conjugate gradient method (CGM) is an efficient iterative regularization technique for solution of the inverse heat conduction problem (IHCP). However, most of the existing CGM schemes deal with linear boundary conditions and constant thermophysical properties. Little attention has been paid to formulate the CGM with radiation boundary condition and temperature-dependent thermophysical properties. In this study, a nonlinear CGM scheme is formulated to recover the front surface heating condition of a 3-D object, based on the temperature measurements at back surface. The 3-D object is subjected to a high-intensity Gaussian laser beam heating on the front surface and a combined radiation and convection boundary condition on the back surface. The derivations of the direct problem, adjoint problem and sensitivity problem are presented in detail. The robustness of the formulated 3-D IHCP algorithm is tested for two materials that are commonly used in aerospace engineering.

Nomenclature

C	volume specific heat, J/(m^3·K)
$d^k(y,z,t)$	direction of descent at iteration k, which is sometimes expressed in vector form $\mathbf{d^k}$
h	convection heat transfer coefficient, W/(m^2·K)
i_m	total number of temperature measurements
k	thermal conductivity, W/(m·K)
L	object length in x direction, m
M	object length in y direction, m
N	object length in z direction, m
q	heat flux, W/m^2
q_{laser}	periodic laser heat flux on front surface, W/m^2
q_{max}	maximum heat flux at the laser Gaussian beam center, W/m^2
$q_1(y,z,t)$	observed heat flux on front surface which is sometimes expressed in vector form $\mathbf{q_1}$, W/m^2
$\Delta q_1(y,z,t)$	heat flux perturbation on front surface
r	radius measured from laser spot center, m
S	objective function
$\nabla S[\mathrm{q}_1^{\mathrm{k}}]$	gradient direction of objective functional at iteration k
$\Delta S[\mathrm{q}_1^{\mathrm{k}}]$	objective function variation
t	time, s
t_f	final time, s
Δt	time step, s
T	temperature, K
T_0	initial temperature, K

[1] Corresponding author. E-mail: zhangyu@missouri.edu

T_∞	ambient temperature, K
$T_1(y,z,t)$	front surface temperature, K
$\Delta T[L,y,z,t;\mathrm{d}^k]$	temperature variation, which is sometimes simplified as ΔT, when the surface heat flux is perturbation is $\Delta q_1(y,z,t)=d^k(y,z,t)$
w	1/e radius of Gaussian laser beam, m
x, y, z	spatial coordinate variables, m
$Y_{TLexact}(y,z,t)$	temperature measurement data without errors on back surface obtained by numerical simulations, K
$Y_{TL}(y,z,t)$	measurement temperature on the back surface, K
Greek symbols	
α	surface absorptivity
β^k	search step size at iteration level *k*
χ	tolerance used to stop the CGM iteration procedure
δ	Dirac delta function
ε	surface emissivity
φ	standard deviation of temperature measurements, K
γ^k	conjugate coefficient at iteration level *k*
$\lambda(x,y,z,t)$	Lagrange multiplier
σ	Stefan-Boltzmann constant, σ =5.67×10^{-8} W/(m^2·K^4)
ω	a random variable having a normal distribution with zero mean and unitary standard deviation
ξ	perturbed variable
Superscripts	
k	iteration level
Subscripts	
0	initial
f	final
q	heat flux
T	temperature

1. Introduction

The inverse heat conduction problems (IHCPs) are mathematically classified as *ill-posed*, so special solution techniques are usually required to transform the ill-posed IHCP into a well-posed one. Although some analytical solutions are available for this purpose (e.g., [1-5]), their application is limited to the IHCPs in one-dimension or simple configuration in 2 or 3 dimensions. For this reason, a number of numerical approaches have been developed for the solution of IHCPs. The interested readers can refer to the books of Tikhonov et al. [6], Beck et al. [7], Alifanov [8] and Özisik [9] for details about these solution technique.

The majority of the numerical methods restate the inverse problem as a least-squares minimization problem over the whole-time domain or in sequential time intervals. Among those, the conjugate gradient method (CGM) has been receiving more and more attentions since it can improve the convergence rate of inverse estimation by choosing the direction of descent as the linear combination of the gradient direction at current iteration with the direction of descent at previous iteration [10]. Due to its excellent self-adjusting, global convergence property, the CGM has been extensively used to solve multidimensional IHCPs (e.g. [11-14]). However, most of the existing CGM algorithms deal with linear boundary conditions and constant thermal properties. Recently, the authors applied the CGM to reconstruct the front-surface heating condition with back-surface heat flux and temperature measurement data [15, 16], but only linear boundary conditions are considered.

To the best of the author's knowledge, little work has been done to formulate the IHCP with radiation boundary

condition and temperature-dependent thermophysical properties. In this study, a 3-D CGM is formulated to reconstruct the front surface heating condition based on the temperature measurement data at the back surface to which a combined radiation and convection boundary condition is imposed. The simulated measurement data are obtained by solving a direct problem in which the front surface is subjected to laser heating as well as convection-radiation cooling and the back surface is subjected to convection-radiation cooling. The results are presented for two materials and excellent agreement between the inverse and exact solutions are demonstrated.

2. Model Description

A three-dimensional object is considered as shown in Fig. 1. Initially, the object is under a uniform temperature T_0 and then is subjected to a high intensity Gaussian laser beam q_{laser} (w is the 1/e radius) on the front surface from $t = 0^+$. The purpose of this study is to demonstrate the effectiveness and accuracy of the proposed IHCP formulation in reconstructing the observed heat flux $q_1(y,z,t)$ and temperature $T_1(y,z,t)$ on the front surface of a 3-D target with temperature-dependent thermophysical properties, based on the measured temperature on the back surface.

2.1 Direct Problem

The direct problem can be expressed as follows:

$$C(T)\frac{\partial T}{\partial t} = \frac{\partial}{\partial x}[k(T)\frac{\partial T}{\partial x}] + \frac{\partial}{\partial y}[k(T)\frac{\partial T}{\partial y}] + \frac{\partial}{\partial z}[k(T)\frac{\partial T}{\partial z}]$$

$$\text{for } 0 < x < L,\ 0 < y < M,\ 0 < z < N,\ t > 0 \tag{1}$$

$$T = T_0 \quad \text{for } 0 \le x \le L,\ 0 \le y \le M,\ 0 \le z \le N,\ t = 0 \tag{2}$$

$$-k(T)\frac{\partial T}{\partial x} = q_1(y,z,t) \quad \text{for } x = 0,\ t > 0 \tag{3}$$

$$-k(T)\frac{\partial T}{\partial x} = h(T - T_\infty) + \varepsilon\sigma(T^4 - T_\infty^4) \quad \text{for } x = L,\ t > 0 \tag{4}$$

$$-k(T)\frac{\partial T}{\partial y} = 0 \quad \text{for } y = 0,\ M;\ t > 0 \tag{5}$$

$$-k(T)\frac{\partial T}{\partial z} = 0 \quad \text{for } z = 0,\ N;\ t > 0 \tag{6}$$

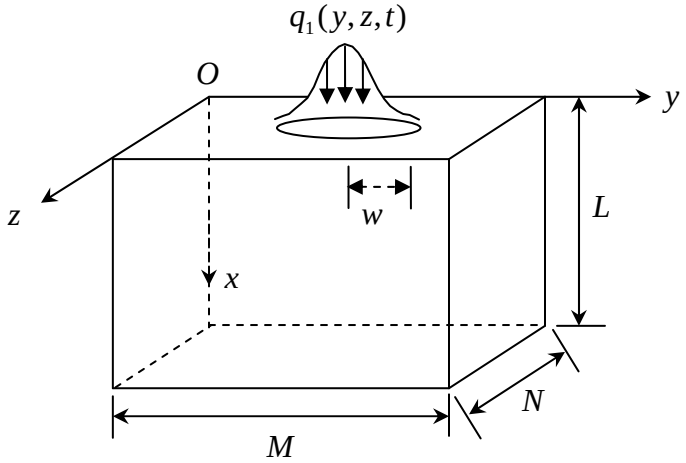

Figure 1 Physical model.

where h, ε and T_∞ are assumed to be constant.

In the direct problem described above, the front-surface heat flux $q_1(y,z,t)$ is considered to be known. The objective of the direct problem here is to determine the transient temperature and heat flux distribution in the target. As can be seen in Eq. (4), the back surface ($x = L$) is subjected to a radiation boundary condition, which makes the heat conduction a nonlinear problem.

2.2 Inverse Problem

For the inverse problem, the heat flux at $x = 0$ is unknown and needs to be recovered, but everything else in the direct problem is known. The additional information needed in the estimation of the front surface heat flux is available from the readings of temperature sensors installed on the back surface. The inverse problem can thus be stated as: the temperature measurements on the back surface, $Y_{TL}(y,z,t)$, is utilized to recover the front surface heat flux. The front surface temperature is computed according to the temperature-heat flux relation defined by the classical Fourier's law.

If the sampling rate of the measurement data is high enough, the data can be approximated as continuous. For this case, the inverse solution can be obtained by minimizing the following ordinary least squares norm:

$$S[\mathbf{q_1}] = \sum_{i=1}^{i_m} \int_0^{t_f} \{Y_{TL}(y_i, z_i, t) - T[L, y_i, z_i, t; \mathbf{q_1}]\}^2 dt \tag{7}$$

where $T[L, y_i, z_i, t; \mathbf{q_1}]$ is the computed heat flux at measuring point i on the back surface.

2.3 Conjugate Gradient Method for Minimization

The iterative process based on the conjugate gradient method (CGM) [8, 9] is now derived below for the estimation of unknown heat flux $q_1(y,z,t)$ by minimizing the objective function S given by Eq. (7). The front surface heat flux $q_1(y,z,t)$ at iteration k+1 is advanced by

$$q_1^{k+1}(y,z,t) = q_1^k(y,z,t) - \beta^k d^k(y,z,t) \tag{8}$$

where β^k is the search step size from iteration k to k+1, which will be addressed in the next section, and $d^k(y,z,t)$ is the direction of descent (i.e. search direction) given by:

$$d^k(y,z,t) = \nabla S[\mathbf{q_1^k}] + \gamma^k d^{k-1}(y,z,t) \tag{9}$$

which is a conjugation of the gradient direction $\nabla S[q_1^k]$ at iteration k and the direction of descent $d^{k-1}(y,z,t)$ at iteration k-1. The conjugate coefficient γ^k is determined by:

$$\gamma^k = \frac{\sum_{i=1}^{i_m} \int_0^{t_f} \nabla S[q_1^k] \cdot \{\nabla S[q_1^k] - \nabla S[q_1^{k-1}]\} dt}{\sum_{i=1}^{i_m} \int_0^{t_f} \{\nabla S[q_1^{k-1}]\}^2 dt} \tag{10}$$

with $\gamma^0 = 0$. To perform the iterations according to Eq. (8), the step size β^k and the gradient of the objective

functional $\nabla S[q_1^k]$ need to be determined. To do so, a *sensitivity problem* and an *adjoint problem* are constructed in the following.

2.4 Sensitivity Problem and Search Step Size

The sensitivity problem is obtained by the application of limiting approach to the boundary and initial conditions of the direct problem. Special care is given to the radiation boundary condition. After some manipulations, the sensitivity problem can be expressed as:

$$\frac{\partial(C\Delta T)}{\partial t}=\frac{\partial^2(k\Delta T)}{\partial x^2}+\frac{\partial^2(k\Delta T)}{\partial y^2}+\frac{\partial^2(k\Delta T)}{\partial z^2}$$

$$\text{for } 0<x<L,\ 0<y<M,\ 0<z<N,\ t>0 \tag{11}$$

$$\Delta T(x,y,z,0)=0 \quad \text{for } 0\le x\le L,\ 0\le y\le M,\ 0\le z\le N,\ t=0 \tag{12}$$

$$-\frac{\partial(k\Delta T)}{\partial x}=\Delta q_1(y,z,t) \quad \text{for } x=0,\ t>0 \tag{13}$$

$$-\frac{\partial(k\Delta T)}{\partial x}=(h+4\varepsilon\sigma T^3)\Delta T \quad \text{for } x=L,\ t>0 \tag{14}$$

$$-\frac{\partial(k\Delta T)}{\partial y}=0 \quad \text{for } y=0,\ M;\ t>0 \tag{15}$$

$$-\frac{\partial(k\Delta T)}{\partial z}=0 \quad \text{for } z=0,\ N;\ t>0 \tag{16}$$

The above equations are to determine the temperature variation $\Delta T(x,y,z,t)$ caused by the perturbation $\Delta q_1(y,z,t)$. It is seen that the boundary condition (14) is related to temperature *T*,, which is essentially caused by the nonlinear boundary condition at *x* = *L*.

After the solution of the sensitivity problem is obtained, the search step size β^k can be determined by minimizing the objective function (Eq.(7)):

$$\beta^k=\frac{\sum_{i=1}^{i_m}\int_0^{t_f}\{T[L,y_i,z_i,t;\mathbf{q_1}]-Y_{TL}(y_i,z_i,t)\}\cdot\Delta T[L,y_i,z_i,t;\mathbf{d^k}]\cdot dt}{\sum_{i=1}^{i_m}\int_0^{t_f}\{\Delta T[L,y_i,z_i,t;\mathbf{d^k}]\}^2\cdot dt} \tag{17}$$

where the temperature $T[L,y_i,z_i,t;q_1]$ is solved from the direct problem (Eqs. (1)~(6)) with the estimated $\mathbf{q_1}$ as the boundary condition at *x* = 0. The sensitivity function $\Delta T[L,y_i,z_i,t;\mathbf{d^k}]$ is the temperature variation at *x* = *L* and time *t*, which is obtained by solving Eqs. (11)~(16) by letting $\Delta q_1(y,z,t)=d^k(y,z,t)$.

2.5 Adjoint Problem and Gradient Equation

To derive the adjoint problem, the least square estimator, Eq. (7), is modified as follows:

$$\begin{aligned}S[\mathbf{q_1}]&=\sum_{i=1}^{i_m}\int_0^{t_f}\{Y_{TL}(y_i,z_i,t)-T[L,y_i,z_i,t;\mathbf{q_1}]\}^2dt\\&+\int_{x=0}^{L}\int_{y=0}^{M}\int_{t=0}^{t_f}\{C(T)\frac{\partial T}{\partial t}-\frac{\partial}{\partial x}[k(T)\frac{\partial T}{\partial x}]-\frac{\partial}{\partial y}[k(T)\frac{\partial T}{\partial y}]-\frac{\partial}{\partial z}[k(T)\frac{\partial T}{\partial z}]\}\lambda dxdydzdt\end{aligned} \tag{18}$$

where $\lambda(x,y,z,t)$ is referred to as Lagrange multiplier.

After the application of limiting process to Eq. (18), we get the following adjoint problem for $\lambda(x,y,z,t)$:

$$C\frac{\partial\lambda}{\partial t}+k\frac{\partial^2\lambda}{\partial x^2}+k\frac{\partial^2\lambda}{\partial y^2}+k\frac{\partial^2\lambda}{\partial z^2}$$

$$+\sum_{i=1}^{i_m}2\{T[x,y_i,z_i,t;\mathbf{q_1}]-Y_{TL}(y_i,z_i,t)\}\delta(x-L)\delta(y-y_i)\delta(z-z_i)=0$$

$$\text{for } 0<x<L,\ 0<y<M,\ 0<z<N,\ t>0 \tag{19}$$

$$\lambda(x,y,z,t_f)=0 \quad \text{for} \quad 0\le x\le L,\ \ 0\le y\le M,\ 0\le z\le N,\ \ t=t_f \tag{20}$$

$$-k\frac{\partial\lambda(0,y,z,t)}{\partial x}=0 \qquad \text{for } x=0,\quad t>0 \tag{21}$$

$$-k\frac{\partial\lambda(0,y,z,t)}{\partial x}=(h+4\varepsilon\sigma T^3)\lambda \qquad \text{for} \quad x=L,\quad t>0 \tag{22}$$

$$-k\frac{\partial\lambda}{\partial y}=0 \quad \text{for} \quad \mathrm{y}=0,\ \ M;\ \ t>0 \tag{23}$$

$$-k\frac{\partial\lambda}{\partial z}=0 \quad \text{for} \quad z=0,\ \ N;\ \ t>0 \tag{24}$$

where $\delta(\cdot)$ is the Dirac delta function. Once again, the temperature T appears in the boundary condition of the adjoint problem (Eq. (22)).

If the Lagrange multiplier $\lambda(x,y,z,t)$ satisfies Eqs. (20)-(24), the modified least square estimator, Eq.(18), can then be simplified as:

$$\Delta S[\mathrm{q}_1]=\int_{z=0}^{N}\int_{y=0}^{M}\int_{0}^{t_f}\lambda(0,y,z,t)\cdot\Delta q_1(y,z,t)dtdydz \tag{25}$$

By assuming that the unknown function $q_1(y,z,t)$ belongs to the Hilbert space of square-integrable functions in the time domain $0<t<t_f$, we can write [9]:

$$\Delta S[\mathrm{q}_1]=\int_{z=0}^{N}\int_{y=0}^{M}\int_{0}^{t_f}\nabla S[q_1(y,z,t)]\cdot\Delta q_1(y,z,t)dtdydz \tag{26}$$

A comparison of Eqs. (25) with (26) leads to the following expression for the gradient of functional $\nabla S[q_1(y,z,t)]$:

$$\nabla S[q_1(y,z,t)]=\lambda(0,y,z,t) \tag{27}$$

2.6 Stopping Criterion

The discrepancy principle is used as the stopping criterion [8, 9]:

$$S[\mathrm{q}_1]<\chi \tag{28}$$

where χ denotes the tolerance. Assume that the absolute value of the heat flux residuals can be approximated by:

$$\left|Y_{TL}(y_i,z_i,t)-T[L,y_i,z_i,t;\mathrm{q}_1]\right|\approx\varphi \tag{29}$$

where φ is the standard deviation of the measurements. Substituting Eq. (29) into Eq. (7), the tolerance χ for the stopping criterion is obtained:

$$\chi=i_m\varphi^2t_f \tag{30}$$

3. Computational Procedure

The solution procedure of the IHCP above using the CGM is summarized as follows. Start with an initial guess $q_1^0(y,z,t)$ for $q_1(y,z,t)$, set $k = 0$, and then perform the steps below:

Step 1. Solve the direct problem given by Eqs. (1)~(6) for $T(x,y,z,t)$ based on the value $q_1^k(y,z,t)$.

Step 2. Check the stopping criterion Eq. (28). Stop the iteration if satisfied; otherwise, continue the following solution procedure.

Step 3. Solve the adjoint problem given by Eqs. (19)~(24) for $\lambda(x,y,z,t)$.

Step 4. Compute the gradient of the objective function $\nabla S[q_1(y,z,t)]$ from Eq. (27).

Step 5. Compute the conjugate coefficient γ^k and the direction of descent $d^k(y,z,t)$ from Eqs. (10) and (9), respectively.

Step 6. Set $\Delta q_1^k(y,z,t) = d^k(y,z,t)$ and solve the sensitivity problem given by Eqs. (11)~(16) for $\Delta T(x,y,z,t)$ and then $\Delta q(x,y,z,t)$.

Step 7. Compute the search step size β^k from Eq. (17).

Step 8. Compute the new estimation for $q_1^{k+1}(y,z,t)$ from Eq. (8) and return to Step 1.

4. Results and Discussion

4.1 Generation of Simulated Measurement Data

Instead of conducting actual experiment, the measurement data of temperature and heat flux are generated numerically from solving the direct problem described by the governing equation (1) with initial condition and boundary conditions at side surfaces given by Eqs. (2), (5), (6) and the following boundary conditions on front and back surfaces

$$-k(T)\frac{\partial T}{\partial x} = q_{laser} - h(T - T_\infty) - \varepsilon\sigma(T^4 - T_\infty^4) \quad \text{for} \quad x = 0, \quad t > 0 \qquad (31)$$

$$-k(T)\frac{\partial T}{\partial x} = h(T - T_\infty) + \varepsilon\sigma(T^4 - T_\infty^4) \quad \text{for} \quad x = L, \quad t > 0 \qquad (32)$$

where h, ε and T_∞ are assumed to be constant as before; q_{laser} is the heat flux imposed on the front surface, which is assumed to be Gaussian type in space:

$$q_{laser}(y,z,t) = q_{\max} \cdot \alpha \cdot \exp\{-[(y - 0.5M)^2 + (z - 0.5N)^2]/w^2\} \qquad (33)$$

which indicates that q_{laser} is centered on the front surface.

By comparing Eqs. (3) and (31), one can see that the relationship between the observed heat flux q_1 and the laser heating flux q_{laser} is:

$$q_1 = q_{laser} - h(T - T_\infty) - \varepsilon\sigma(T^4 - T_\infty^4)$$

In the inverse heat transfer analysis, the simulated back surface temperature is used as the measurement data and employed in the objective function. The recovered front-surface heat flux and temperature will be compared

with those calculated from the above direct problem (i.e. Eqs.(1), (2), (5), (6), (31) and (32)) to examine the accuracy of the present inverse heat conduction algorithm.

If not otherwise specified, the back-surface simulated measurement data obtained from Eqs. (1), (2), (5), (6), (31) and (32) will be directly used as the temperature measurement data in the inverse solution since temperature can be measured with high accuracies [17, 18]. Nevertheless, the effects of the uncertainties in temperature measurements on the accuracy of the inverse solution will be examined to demonstrate the robustness of the formulated algorithm. For this purpose, we add an error term to $Y_{TLexact}(y,z,t)$ in the form:

$$Y_{TL}(y,z,t) = Y_{TLexact}(y,z,t) + \omega\varphi \tag{34}$$

where $Y_{TLexact}(y,z,t)$ is the simulated measurement data (errorless) obtained from the direct problem described by Eqs. (1), (2), (5), (6), (31) and (32); φ is the standard deviation of the measurements can be an absolute temperature value or be set as a percentage of the highest temperature value on the back surface; ω is a random variable with normal distribution with zero mean and unitary standard deviation. The measurement data obtained by Eq. (34) contain random errors that have a normal distribution with standard deviation equal to φ.

4.2 Results of IHCP

The numerical analyses presented in this study are performed for Stainless Steel 304 and Aluminum Alloy 2024-T6, which are commonly used in aerospace engineering. Their temperature-dependent thermophysical properties [19] are plotted in Figs. 2. When the highest temperature exceeds the maximum temperature at which thermophysical properties are available, the thermophysical properties are obtained by linear extrapolation. Other simulation parameters are: L = 2.5 mm, M = 68.4 mm, N = 68.4 mm, T_0 = 300 K, T_∞ = 300 K, h =5 W/(m^2 • K), $\varepsilon = 0.92$. The parameters for the front surface heat flux are assumed to be: $q_{\max}$ = 4000 W/cm^2, w = 7.6 mm. The control volume method [20] is used to solve the direct problem, sensitivity problem and adjoint problem. Time discretization is obtained by applying a fully implicit scheme. The grid numbers along the y- and z-direction are 13×13, while the grid number along the x-direction is 9. The final time is chosen as $t_f = 1.6\ s$, and the time step $\Delta t = 0.1\ s$. Therefore, a total number of 1936 unknown discrete heat flux data are to be determined in the present study.

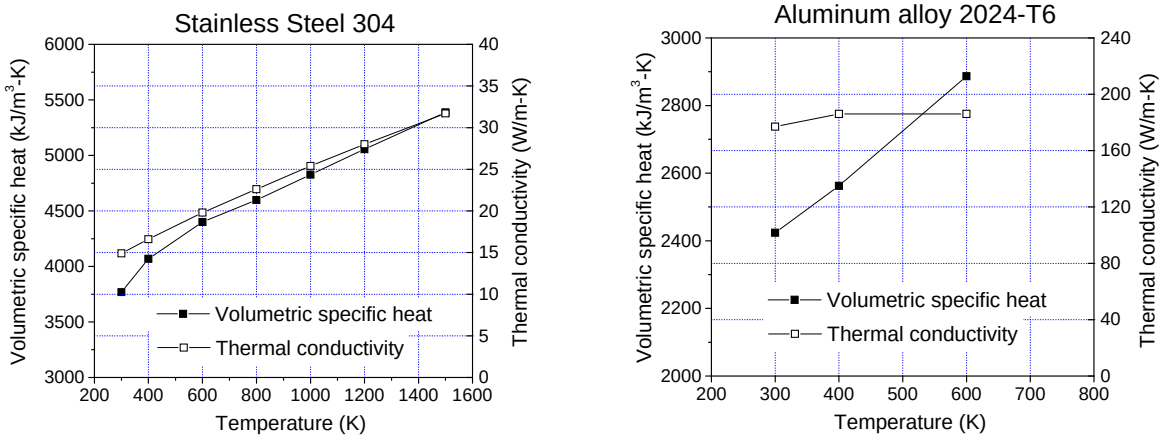

(a) (b)

Figure 2 Thermal properties of stainless Steel 304 and Aluminum Alloy 2024-T6 [19].

The locations of temperature sensors are schematically shown in Figure 3, in addition to the finite difference mesh on the back surface. The dash lines represent the faces of control volumes. As seen in Fig. 3, a non-uniform grid system is adopted with a denser mesh around the laser spot center for capturing the drastic thermal response in this region. The solid triangles represent the sensor locations, which coincide with the centers of the control volumes (i.e., the locations of grid points). The red circle in Fig. 3 is the 1/e radius of the Gaussian laser beam. A total number of 121 temperature sensors are attached to the back surface to provide additional information in recovering the front surface heating condition.

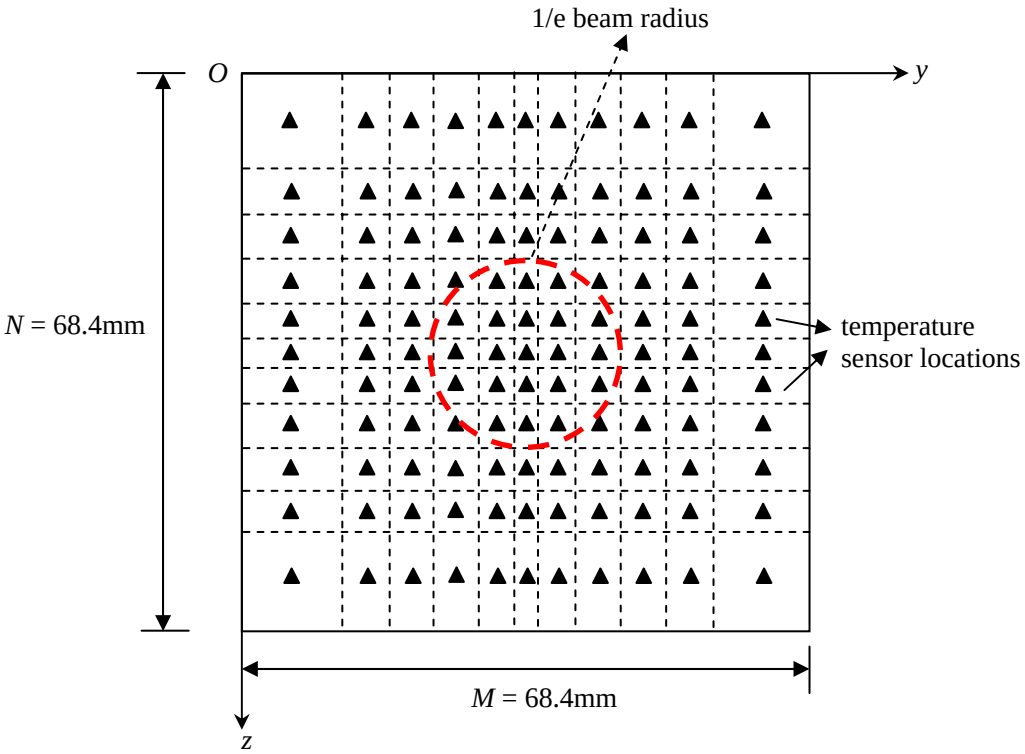

Figure 3 Locations of temperature sensors on the back surface.

Figures 4-7 present the inverse simulating results when the back-surface temperature measurement data are considered to be errorless. Figure 4 shows the recovered heat fluxes (as mentioned before, the recovered heat flux in this paper means the observed heat flux q_1) and temperatures at the spot center and at the radius r = 13.4 mm for stainless steel AISI 304. The surface absorptivity is set as α = 0.05. The exact solutions are obtained by solving the direct problem described by Eqs. (1), (2), (5), (6), (31) and (32). As shown in Fig. 4, both the temperature and heat flux at the spot center and r = 13.4 mm can be well recovered. The root mean square (RMS) difference shown in Fig. 4 is defined as:

$$RMS = \sqrt{\frac{1}{n}\sum_{i=1}^{n}(A_i - B_i)^2} \qquad (35)$$

where A and B are any two quantities to be compared; n is the total number of sample points.

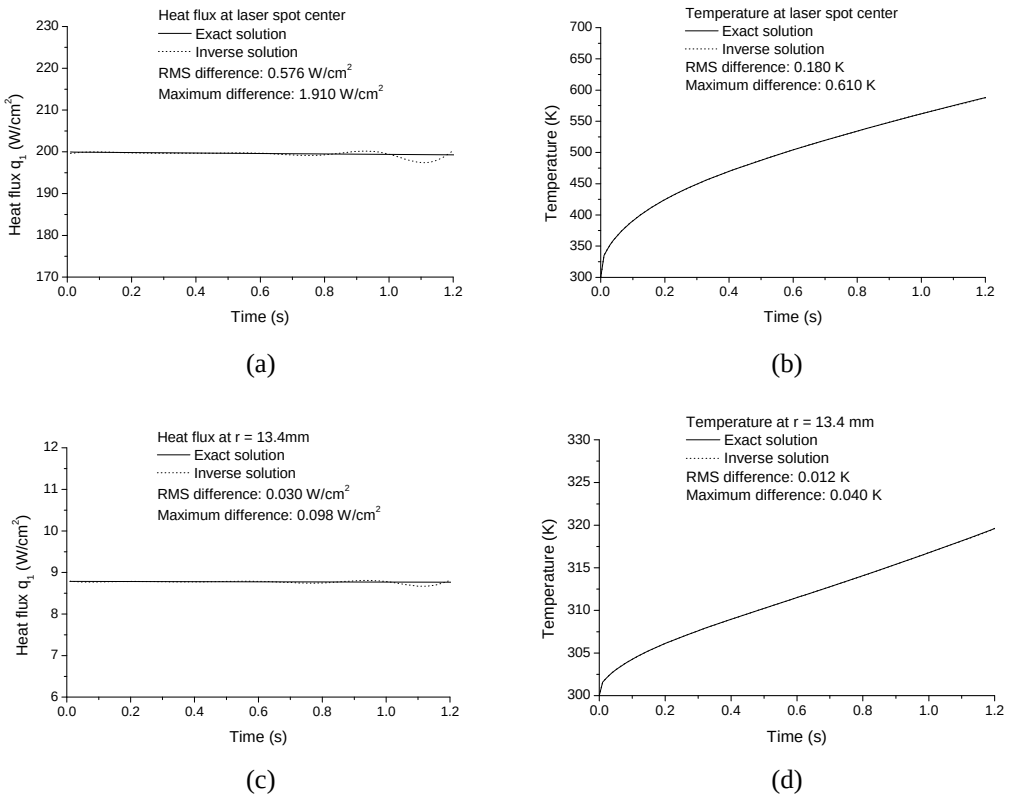

Figure 4 Recovered heat fluxes and temperatures at the spot center and at the radius *r* = 13.4 mm for stainless steel AISI 304. (a) Recovered heat flux at the laser spot center; (b) Recovered temperature at the laser spot center; (c) Recovered heat flux at the radius *r* = 13.4 mm; (d) Recovered temperature at the radius *r* = 13.4 mm.

Figure 5 displays the 2-D contour distributions of the recovered heat fluxes and temperatures at front surface (x = 0) at the time of 0.8 s. It can be seen in Fig. 5 that the heat fluxes and temperatures can be accurately reconstructed everywhere over the entire front surface using the present numerical algorithm.

Figure 6 presents the recovered heat fluxes and temperatures at the laser spot center and at the radius r = 13.4 mm for Aluminum 2024-T6. The surface absorptivity is α = 0.018. It is observed in Fig. 6 that both the recovered heat flux and temperature at the front surface are in excellent agreement with the exact results.

Figure 7 shows the 2-D contour distributions of the recovered heat fluxes and temperatures for Al2024-T6 at the time of 0.8 s. It is clearly shown that the 2-D distributions of the heat flux and temperature over the entire front surface can also be accurately reconstructed in high resolution.

In the foregoing discussions, the temperature measurement data on the back surface are assumed to be errorless. In reality, measurement errors are unavoidable. Figure 8 investigates the influence of error-containing temperature measurements on the accuracy of the inverse solutions for stainless steel AISI 304. Other simulation parameters are the same as those in Fig.4. The standard deviation φ of the temperature measurements is assumed to be 0.5K, 1K, 2K and 5K. It can be seen in Figs. 8 (a) and (c) that when the temperature measurements contain φ =5 K errors, the relative RMS errors in the heat flux estimations are about 4.71% and 28.99% at the laser spot center and at r = 13.4mm, respectively. This indicates that the heat flux within the region around the laser spot center can still be

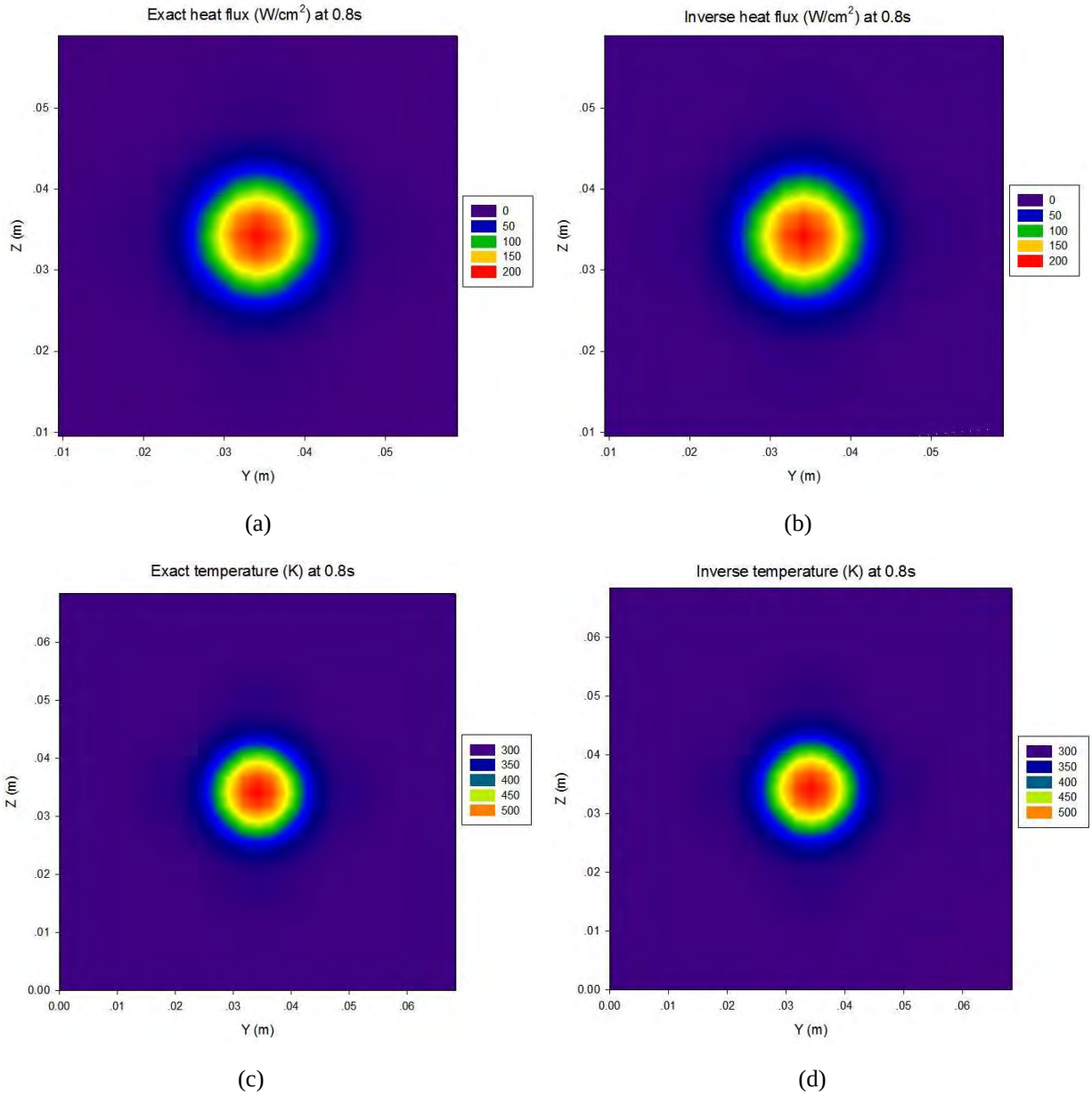

Figure 5 2-D distributions of the recovered heat fluxes and temperatures for stainless steel AISI 304 at *t* = 0.8 s. (a) Exact heat flux distribution; (b) Recovered heat flux distribution; (c) Exact temperature distribution; (d) Recovered temperature distribution.

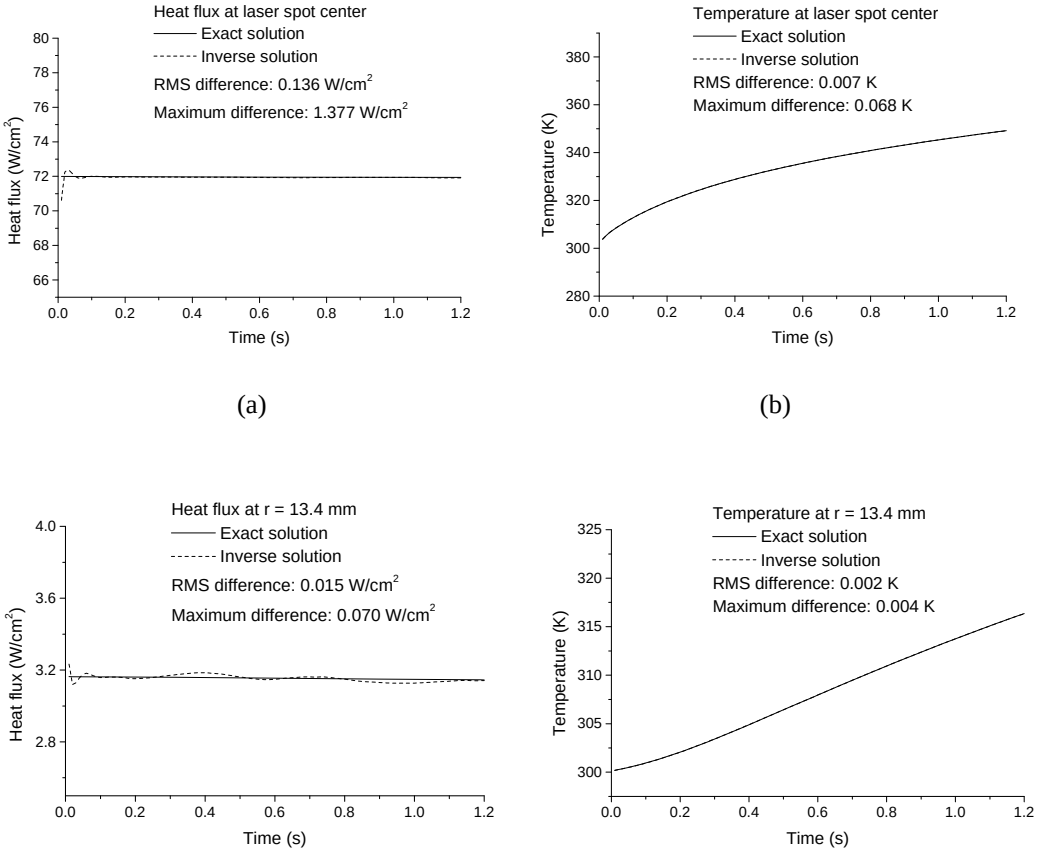

Figure 6 Recovered heat fluxes and temperatures at the spot center and at the radius r = 13.4 mm for Al 2024-T6. (a) Recovered heat flux at the laser spot center; (b) Recovered temperature at the laser spot center; (c) Recovered heat flux at the radius r = 13.4 mm; (d) Recovered temperature at the radius r = 13.4 mm.

recovered in an acceptable accuracy, but there is pronounced degradation in the heat flux estimation outside the laser spot region. However, it is seen in Figs. 8 (b) and (d) that even when the random errors in the temperature measurements are as high as 5K, the temperatures can still be reconstructed in a high accuracy no matter which region is considered. This shows that the inverse formulation developed in this study is very robust in recovering the front-surface temperature. This is very important since the temperature, not the heat flux, will be used as the input information when the subsequent thermomechanical analysis is performed to explore the damage mechanism.

5. Conclusions

A nonlinear conjugate gradient method (CGM) algorithm is formulated to recover the heat flux and temperature at the front (heated) surface of a 3-D object with temperature-dependent thermophysical properties and radiation boundary condition, based on the temperature measurements on the back surface (opposite to the heated surface). The inverse problem is formulated in such a way that the front-surface heat flux is chosen as the unknown function to be recovered, and the front-surface temperature is computed as a by-product of the IHCP algorithm. It is shown

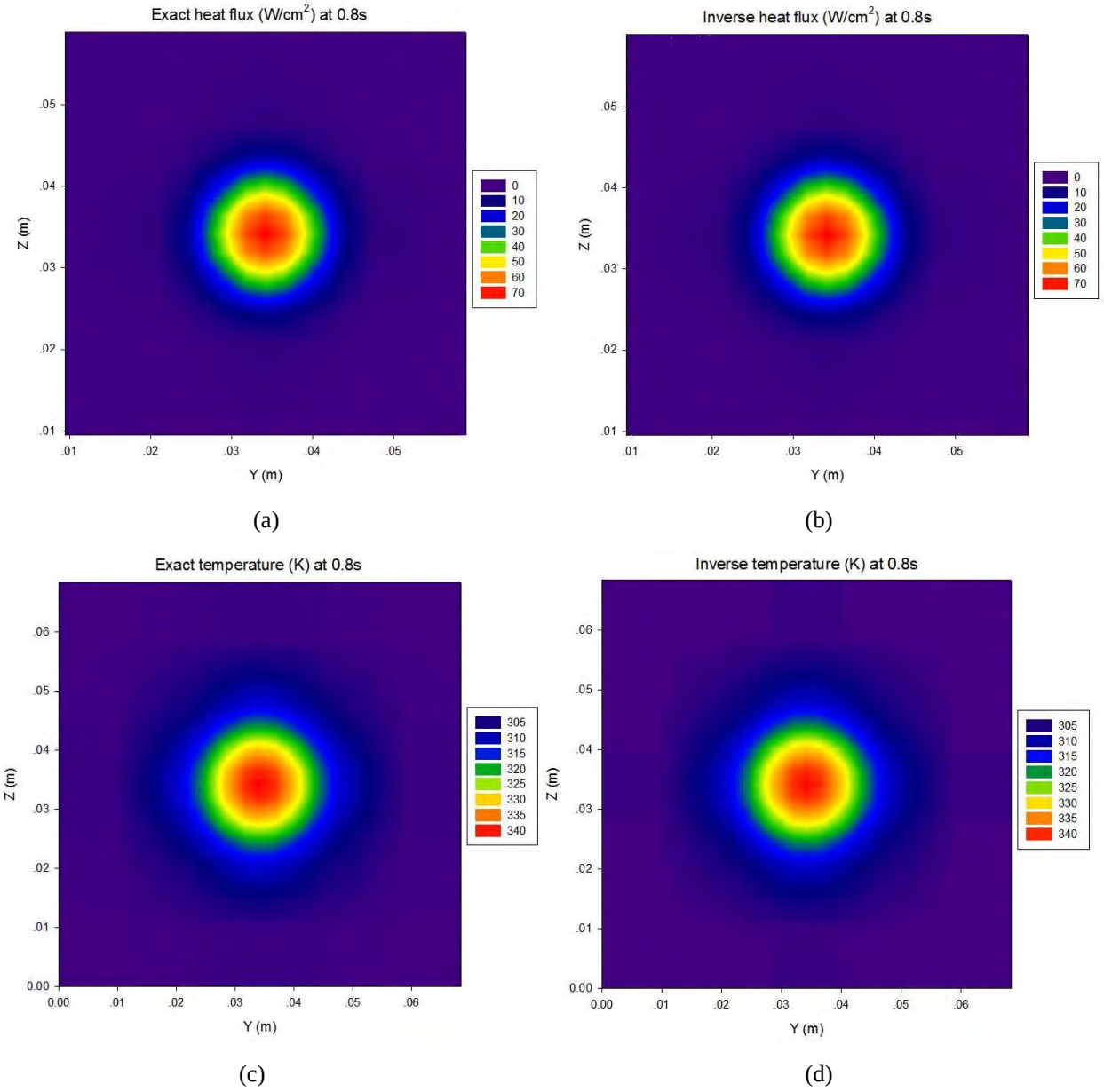

Figure 7 2-D distributions of the recovered heat fluxes and temperatures for Al 2024-T6 at t = 0.8 s. (a) Exact heat flux distribution; (b) Recovered heat flux distribution; (c) Exact temperature distribution; (d) Recovered temperature distribution.

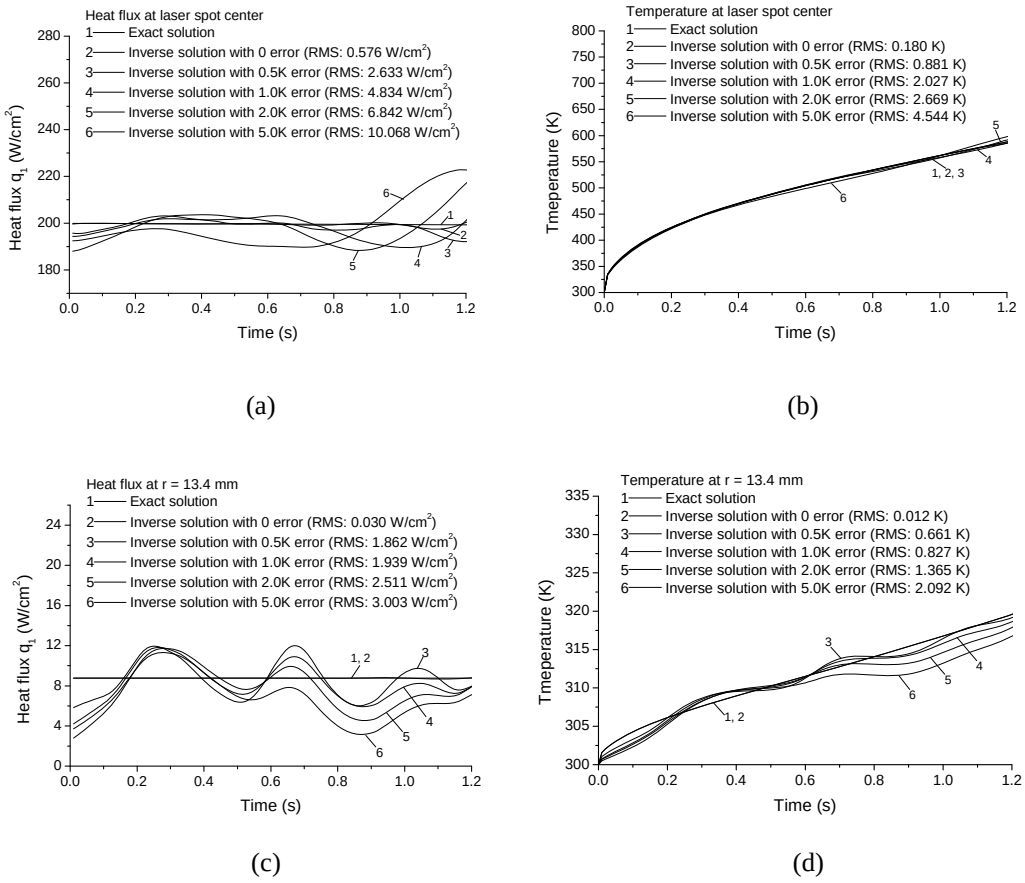

Figure 8 Influence of the random errors in temperature measurements on the back surface on the accuracies of the inverse solutions for stainless steel AISI 304. (a) Recovered heat flux at the laser spot center; (b) Recovered temperature at the laser spot center; (c) Recovered heat flux at the radius *r* = 13.4 mm; (d) Recovered temperature at the radius *r* = 13.4 mm.

that, due to the presence of the radiation boundary condition, the mathematical formulations of the adjoint and sensitivity problems are different from those just involving pure linear boundary conditions. Numerical simulations are conducted to test the performance of the developed inverse model for two materials, which have wide applications in aerospace engineering, heated by a high-intensity Gaussian laser beam. The results show that the 2-D heat flux and temperature distributions on the front surface can be excellently reconstructed when the temperature measurements contain small random errors. The influence of temperature measurements with large errors on the accuracy of the inverse solutions is also examined. It is found that when the random errors in the temperature measurements are as high as 5 K, the recovered heat flux was much less accurate than the recovered temperature, but the recovered temperatures can still be reconstructed in a satisfied accuracy. This shows that the inverse formulation developed in this study is very robust in recovering the front-surface temperature based on the temperature measurements on the back surface.

Acknowledgement

The authors would like to thank the Test Resource Management Center (TRMC) Test and Evaluation/Science & Technology (T&E/S&T) Program for their support. This work is funded by the T&E/S&T Program through the U.S. Army Program Executive Office for Simulation, Training and Instrumentation's contract number W900KK-08-C-0002. The authors would also like to express their gratitude to Dr. James L. Griggs for his valuable discussions.

References

[1] Burggraf, O. R., "An exact solution of the inverse problems in heat conduction theory and application," *ASME Journal of Heat Transfer*, Vol. 86, 1964, pp. 373-382.

[2] Langfor, D., "New analytical solutions of the one-dimensional heat equation for temperature and heat flow rate both prescribed at the same fixed boundary (with applications to the phase change problem)," *Quarterly of Applied Mathematics*, Vol. 24, 1976, pp. 315-322.

[3] Aviles-Ramos, C., Haji-Sheikh, A., and Beck, J. V., "Exact solution of heat conduction in composite materials and application to inverse problems," *ASME Journal of Heat Transfer*, Vol. 120, 1998, pp. 592-599.

[4] Monde, M., "Analytical method in inverse heat transfer problem using Laplace transform technique," *International Journal of Heat and Mass Transfer*, Vol. 43, 2000, pp. 3965-3975.

[5] Segall, A. E., "An inverse solution for determining arbitrary boundary-conditions using a least-square approach," *ASME Journal of Heat Transfer*, Vol. 127, 2005, pp. 1403-1405.

[6] Tikhonov, A. N., and Arsenin, V. Y., *Solution of Ill-Posed Problems*, Winson, Washington, D.C., 1977.

[7] Beck, J. V., Blackwell, B., and St-Clair, C. R., *Inverse Heat Conduction: Ill Posed Problems*, Wiley, New York, 1985.

[8] Alifanov, O. M., *Inverse Heat Transfer Problems*, Springer-Verlag, Berlin/Heidelberg, 1994.

[9] Özisik, M. N., and Orlande, H. R. B., *Inverse Heat Transfer: Fundamentals and Applications*, Taylor & Francis, New York, 2000.

[10] Colaco, M. J., Orlande, H. R. B., and Dulikravich, G. S., "Inverse and optimization problems in heat transfer," *Journal of the Brazilian Society of Mechanical Sciences and Engineering*, Vol. XXVIII, No. 1, 2006, pp. 1-24.

[11] Xue, X., Luck, R., and Berry, J. T., " Comparisons and improvements concerning the accuracy and robustness of inverse heat conduction algorithms," *Inverse Problems in Science and Engineering*, Vol. 13, No. 2, 2005, pp. 177-199.

[12] Huang, C. H., and Wang, S. P., "A three-dimensional inverse heat conduction problem in estimating surface heat flux by conjugate gradient method," *International Journal of Heat and Mass Transfer*, Vol. 42, 1999, pp. 3387-3403.

[13] Loulou, T, and Scott, E. P., "An inverse heat conduction problem with heat flux measurements," *International Journal for Numerical Methods in Engineering*, Vol. 67, 2006, pp. 1587-1616.

[14] Abboudi, S., and Artioukhine, E., "Parametric study and optimal algorithm of a simultaneous estimation in two-dimensional inverse heat conduction problem," *Inverse Problems in Science and Engineering*, Vol. 16, No. 4, 2008, pp. 461-482.

[15] Zhou, J., Zhang, Y., Chen, J. K., and Feng, Z. C., "Inverse heat conduction using measured back surface temperature and heat flux," *AIAA Journal of Thermophysics and Heat Transfer*, Vol. 24, No. 1, 2010, pp. 95-103.

[16] Zhou, J., Zhang, Y., Chen, J. K., and Feng, Z. C., “Inverse estimation of surface heating condition in a three-dimensional object using conjugate gradient method,” *International Journal of Heat and Mass Transfer,* Vol. 53, No. 13-14, 2010, pp. 2643-2654.

[17] Tong, A., “Improving the accuracy of temperature measurements,” *Sensor Review*, Vol. 21, No. 3, 2001, pp. 193-198.

[18] Childs, P. R. N., “Advances in temperature measurement,” *Advances in Heat Transfer*, Vol. 36, 2002, pp. 111-181.

[19] Incropera, F. P., Dewitt, D. P., Bergman, T. L., and Lavine, A. S., *Fundamentals of Heat and Mass Transfer*, 6th Ed., John Wiley & Sons, New York, 2007.

[20] Patankar, S. V., *Numerical Heat Transfer and Fluid Flow*, Hemisphere Publishing Corp., New York, 1980.